



# Experimental investigation and thermodynamic assessment of Al–Ca–Ni ternary system

Yurong Jiang<sup>1</sup>, Xi Shi<sup>1</sup>, Xiaoheng Bao<sup>1,2</sup>, Ye He<sup>1</sup>, Shuaixiong Huang<sup>1</sup>, Di Wu<sup>1</sup>, Weimin Bai<sup>1</sup>, Libin Liu<sup>1,\*</sup>, and Ligang Zhang<sup>1,\*</sup>

<sup>1</sup> School of Materials Science and Engineering, Central South University, Changsha 410083, Hunan, People's Republic of China

<sup>2</sup> State Key Laboratory of Powder Metallurgy, Central South University, Changsha 410083, Hunan, People's Republic of China

Received: 3 February 2017

Accepted: 29 June 2017

Published online:  
17 July 2017

© Springer Science+Business  
Media, LLC 2017

## ABSTRACT

The Al–Ca–Ni ternary system has been experimentally investigated and thermodynamically assessed to contribute to the development of a novel Al-base amorphous alloy. A new approach in alloy preparation was used due to the special properties of calcium. With selected equilibrated alloys, the isothermal sections of the Al–Ca–Ni system at 873 and 673 K were obtained by means of scanning electron microscopy, electron probe micro-analysis (EPMA) and powder X-ray diffractometry (XRD). Phase transformation temperatures were measured by differential scanning calorimetry (DSC) analysis. The liquidus projection of this ternary system was determined by identification of primary crystallization phases in as-cast samples and from the liquidus temperatures obtained from DSC analysis. A new ternary compound  $\text{Al}_{78}\text{Ca}_9\text{Ni}_{13}$  (referred to as  $\tau_3$  here after) has been confirmed to exist in both the 873 and 673 K isothermal sections on the basis of EPMA and XRD analysis. All sample compositions are Al-rich: A1–A4 samples > 72.64 at.% Al, B1–B10, C1–C11 > 45 at.% Al, with only C12 at 36.8 at.% Al. Based on the available data of the binary systems Al–Ni, Al–Ca, Ca–Ni and the ternary system Al–Ca–Ni from the literature and present work, thermodynamic modelling of the Al–Ca–Ni ternary system was performed using the calculation of phase diagram method coupled with first-principle calculations. A set of consistent thermodynamic parameters for the Al–Ca–Ni ternary system was obtained with good agreement with the experimental results in the Al-rich region. The calculated data in the Al-poor region are a very plausible prediction, but not validated.

## Introduction

Bulk Al-based amorphous alloys have been brought into focus due to their low density, high specific strength and excellent corrosion, abrasive resistance,

etc. [1–4]. However, the main obstacle for applications of Al-based amorphous alloys was its limiting glass-forming ability (GFA). GFA is vital to develop novel bulk metallic glass (BMG). Due to the unique properties of Al-based amorphous alloys systems,

Address correspondence to E-mail: pdc@csu.edu.cn; ligangzhang@csu.edu.cn

many empirical rules, which have been successfully used in prediction of the GFA of the other metal-based amorphous alloys, such as deep eutectic and the confusion principle, are ineffective in the prediction of the GFA in Al-based amorphous alloys systems. In order to reasonably predict the GFA of Al-based glass, new rules with more sound scientific background must be proposed. GFA can be characterized as scaling inversely with the cooling rate ( $R_c$ ) necessary to avoid crystallization in the alloy system [5]. However, the critical cooling rate for glass formers, like Al-based alloys, was difficult for measurement [6]. Combining the thermodynamic and kinetic calculation can be a more scientific approach to obtaining  $R_c$  and then predict the GFA of Al-based metallic glass alloys [7].

Wang et al. [8] reported that the thermal stability and the GFA of Al-based metallic glasses are enhanced greatly by proper Ca addition. Ayers et al. [9] reported that Al-base amorphous alloys containing 7.5 at.% Ca and 2.5–5 at.% Ni exhibit strength levels which were comparable to some commercial alloys. Minor Ca substitution for Al was examined to retard the precipitation of Fcc<sub>Al</sub> [8]. The mixed Al and glassy phase are extended in a wide heating temperature range, which was favourable for the development of high-strength nanostructure Al-based bulk alloys [10].

The phase diagram is a basic guidance for selection of alloy composition with glass-forming ability [11–16]. In this work, the Al–Ca–Ni ternary system has been systematically studied through experimental investigation and thermodynamic modelling. Isothermal sections at 673 and 873 K, liquidus projection, invariant reaction temperatures were obtained, and a set of self-consistent thermodynamic parameters of this system was also established by means of the CALPHAD approach [17]. These thermodynamic parameters can be used to predict the GFA of Al–Ca–Ni system.

## Literature review

### Binary systems

The first systematic investigation of the Al–Ni phase diagram was reported by Alexander and Vaughan [18] using cooling curve arrests and optical metallography. Subsequently, Nash et al. [19] re-

investigated this system based on the data produced by Alexander and Vaughan [18]. The phase diagram proposed by Nash et al. [19] was further revised by Okamoto [20] and is now the standard for Al–Ni phase diagram. The phase diagram of the Al–Ni system was first calculated with the help of the CALPHAD method by Kaufman and Nesor [21]. They considered the B2 phase to be disordered with the Bcc<sub>A2</sub> structure. In 1996, Du and Clavaguera [22] used two different models for the Fcc (Al, Ni) phase and ordered L12 (AlNi<sub>3</sub>) phases to model the Al–Ni system. After that, Ansara et al. [23] modelled the Fcc phase in the disordered state, Fcc (Al, Ni), and in the ordered state, L<sub>12</sub> (AlNi<sub>3</sub>), using a compound energy model [24] with two sublattices. However, the short-range order (SRO) in the lattice was ignored. Subsequently, Huang and Chang [25] summarized the early work and re-evaluated this phase diagram. In 2001, Dupin et al. [26] used the substitutional solution model for the liquid, Bcc and Fcc phases and the order–disorder relations with a two sublattice model that were applied to the ordered Bcc phase (AlNi) and the ordered Fcc phase (AlNi<sub>3</sub>). Zhang et al. [27] improved the assessment of Huang and Chang [25] by introducing the cluster site approximation for the evaluation of the stability of stable and metastable Fcc ordered phases. In 2011, based on new experiments regarding heat capacity of Al<sub>3</sub>Ni phase, Chen et al. [28] reassessed this binary system but did not use order–disorder relations for the Fcc and Bcc phases. Recently, Wang and Cacciamani [29] evaluated the Al–Ni binary system based mainly on the result of Dupin et al. [26] and added a binary compound (Al<sub>4</sub>Ni<sub>3</sub>). However, this phase is absent in most published Al–Ni phase diagrams, and this phase could not be determined experimentally by Wang and Cacciamani [29]. The thermodynamic parameters from Dupin et al. [26] were adopted in present work.

The Al–Ca phase diagram reported by Hansen and Anderko [30] with the two confirmed binary compounds, Al<sub>2</sub>Ca and Al<sub>4</sub>Ca, has been accepted as a complete phase diagram for a long time. However, most recent studies [31, 32] have indicated that there two more compounds exist in this system, Al<sub>14</sub>Ca<sub>13</sub> and Al<sub>3</sub>Ca<sub>8</sub> whose crystal structure was investigated and well defined by X-ray diffraction techniques. Ozturk et al. [33] assessed the Al–Ca system thermodynamically using the random solution model and the associated model. Wolverton et al. [34] have

shown that the first-principle calculations may provide key formation energies data of the intermetallic phase and hence be used as a useful complement to experimental information in the CALPHAD approach. Recently, Ozturk et al. [35] reassessed the Al–Ca system with both experimental data and first-principle calculation data. The thermodynamic parameters from their recent work were adopted in this work.

Takeuchi et al. [36] reported a phase diagram from differential thermal analysis (DTA) with a congruent melting point at  $\text{CaNi}_5$  and a eutectic line between this compound and Ni-Fcc. Buschow [37] later determined the existence of the four intermetallic compounds with  $\text{CaNi}_2$ -cubic,  $\text{CaNi}_3$ -rhombohedral,  $\text{Ca}_2\text{Ni}_7$ -rhombohedral and  $\text{CaNi}_5$ -hexagonal crystal structure by X-ray diffraction. However, a later work by Saindrean et al. [38] supposed that the melting of  $\text{CaNi}_5$  occurs through a peritectic transformation. In

order to clarify this, a series of experiments by DTA on the Ni-rich part were carried out by Notin et al. [39] and confirmed the congruent melting of  $\text{CaNi}_5$  and found the eutectic point between  $\text{CaNi}_5$  and Ni. Based on the experimental results [39], the Ca–Ni binary system has been optimized by Uremovich et al. [40], which was adopted in this present work.

Three binary phase diagrams [26, 35, 40] were adopted in this present work and are illustrated in Fig. 1. The crystallographic data of all the compounds in the ternary Al–Ca–Ni system are listed in Table 1.

### Ternary system

According to the early work of Shinoda [41], a ternary eutectic reaction occurs in the Al-rich region of the Al–Ca–Ni system. The eutectic reaction  $L \rightarrow \text{Al} + \text{Al}_3\text{Ni} + \text{Al}_4\text{Ca}$  occurs at 883 K and 4.8 at.% Ca and 2.8 at.% Ni. The discovery of a ternary compound

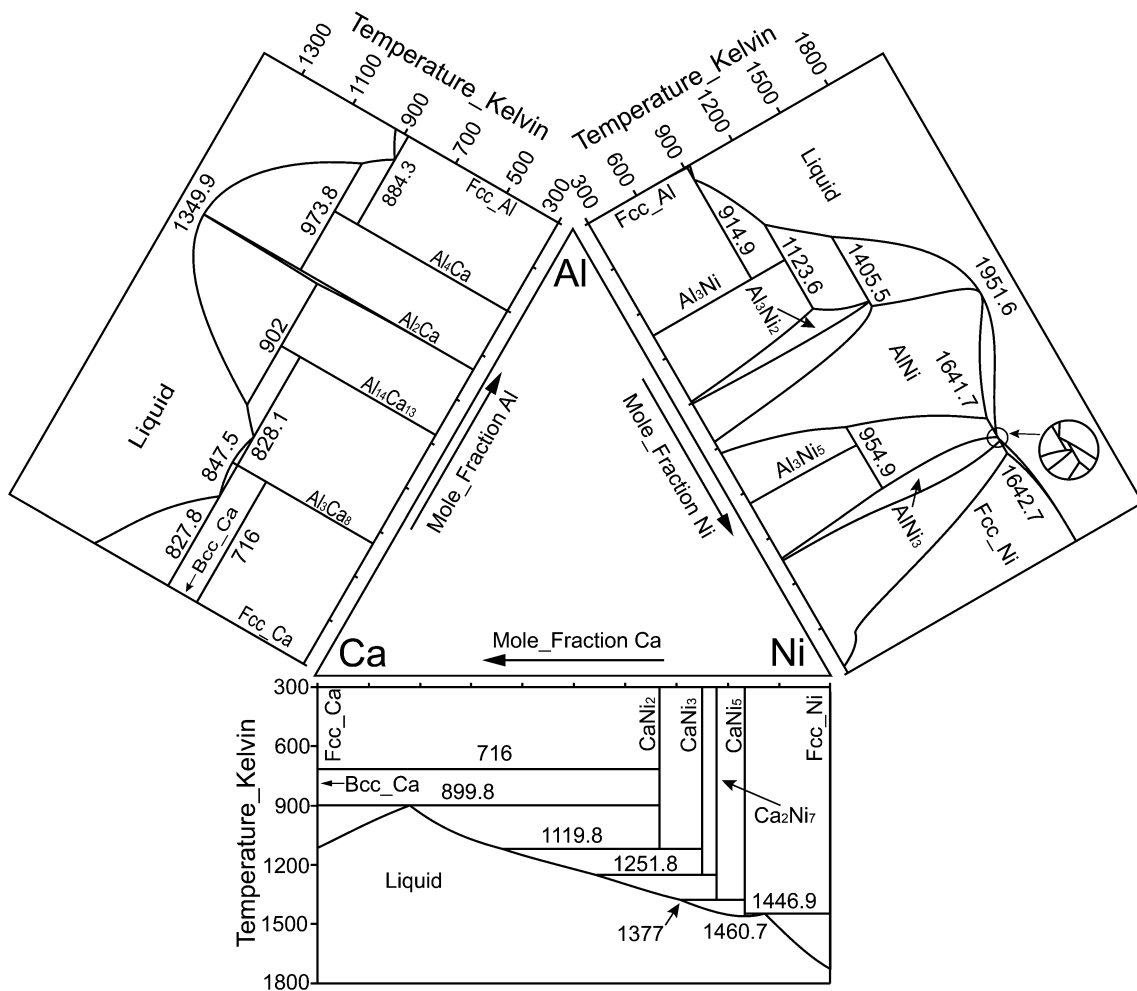


Figure 1 Calculated binary phase diagrams of Al–Ni [26], Al–Ca [35] and Ca–Ni [40] systems.

**Table 1** Crystallographic data of solid phases in the Al–Ca–Ni ternary system

Phase	Lattice parameters			Phase prototype, Pearson symbol, space group	References
	a (nm)	b (nm)	c (nm)		
Al	0.40488	0.40488	0.40488	Cu, cF4, Fm-3 m (225)	[44]
Ca (>716 K)	0.45	0.45	0.45	W, cI2, Im-3 m (227)	[44]
Ca (<716 K)	0.5565	0.5565	0.5565	Cu, cF4, Fm-3 m (225)	[44]
Al <sub>4</sub> Ca	0.4353	0.4353	1.107	Al <sub>4</sub> Ba, tI10, I4/mmm (139)	[45]
Al <sub>2</sub> Ca	0.804	0.804	0.804	MgCu <sub>2</sub> , cF24, Fd-3 m (227)	[45]
Al <sub>14</sub> Ca <sub>13</sub>	1.5551	0.9873	0.9726	Al <sub>14</sub> Ca <sub>13</sub> , mC54, C2/m1 (12)	[31]
Al <sub>3</sub> Ca <sub>8</sub>	0.9484	0.9592	0.9671	In <sub>3</sub> Ca <sub>8</sub> , aP22, P63/P-1 (2)	[31]
Ni	0.354	0.354	0.354	Cu, cF4, Fm-3 m (225)	[44]
Al <sub>3</sub> Ni	0.6613	0.7367	0.4811	Fe <sub>3</sub> C, oP16, Pnma (62)	[46]
Al <sub>3</sub> Ni <sub>2</sub>	0.4028	0.4028	0.4891	Al <sub>3</sub> Ni <sub>2</sub> , hP5, P-3m1 (164)	[44, 45]
AlNi	0.28866	0.28866	0.28866	CsCl, cP2, Fm-3 m (221)	[44]
Al <sub>3</sub> Ni <sub>5</sub>	0.753	0.661	0.376	Ga <sub>3</sub> Pt <sub>5</sub> , oS16, Cmmm (65)	[44]
AlNi <sub>3</sub>	0.3561	0.3561	0.3561	Cu <sub>3</sub> Au, cP4, Pm-3 m (221)	[44]
CaNi <sub>2</sub>	0.7251	0.7251	0.7251	MgCu <sub>2</sub> , cF24, Fd-3 m (227)	[37]
Ca <sub>2</sub> Ni <sub>7</sub>	0.5009	0.5009	3.606	Gd <sub>2</sub> Co <sub>7</sub> , hR54, R-3mh (166)	[37]
CaNi <sub>3</sub>	0.5030	0.5030	0.5030	PuNi <sub>3</sub> , hR36, R-3mh (166)	[47]
CaNi <sub>5</sub>	0.4955	0.4955	0.4955	CaCu <sub>5</sub> , hP6, P6/mmm (191)	[48]
τ <sub>1</sub>	0.76002	0.76002	0.79457	Al <sub>9</sub> CaNi, hP22, P63/mmc (194)	[42]
τ <sub>2</sub>	1.2532	1.450	0.3975	Al <sub>8</sub> Fe <sub>2</sub> Ce, oP44, Pbam (55)	[43]
τ <sub>3</sub>	–	–	–	–	This work

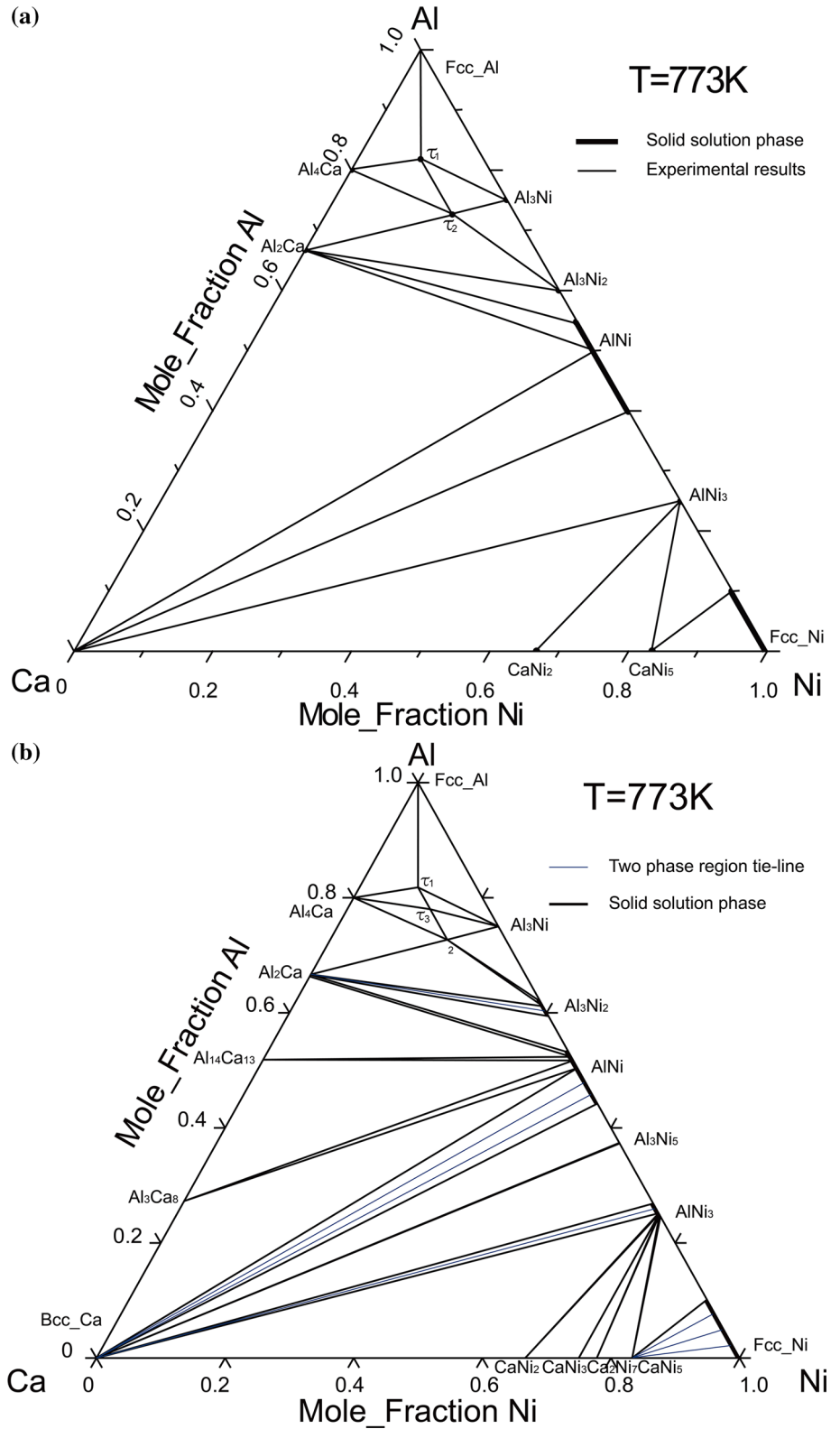
Al<sub>9</sub>CaNi (named τ<sub>1</sub> here after) [42] implies that the ternary eutectic reaction detected by Shinoda [41] probably involves the formation of Al + Al<sub>4</sub>Ca + Al<sub>9</sub>CaNi at 883 K. Manyako et al. [43] reported the 773 K isothermal section of the Al–Ca–Ni system (Fig. 2a) including two ternary compounds, Al<sub>9</sub>CaNi and Al<sub>8</sub>CaNi<sub>2</sub> (named τ<sub>2</sub> here after), and their crystallographic data were also reported [42, 43]. There is little solubility of Ca in the binary Al–Ni phases or of Ni in the binary Al–Ca phases. According to the Al–Ni [26] binary phase diagram, the change of the component of Ni in the homogeneity region of AlNi solid solution was 46.91–55.94 at.% Ni at 773 K. However, the 773 K isothermal section reported by Manyako et al. [43] displayed the composition region of AlNi was 45–60 at.% Ni. The Al<sub>3</sub>Ni<sub>2</sub> and AlNi<sub>3</sub> were solid solution phases, while they were treated as stoichiometric phases in the result of Ref. [43]. According to Manyako et al. [43], Al<sub>3</sub>Ni<sub>5</sub> could not be observed in the isothermal section of the Al–Ca–Ni ternary system at 773 K. However, the compound Al<sub>3</sub>Ni<sub>5</sub> could stably exist at 773 K according to the Al–Ni [26] binary phase diagram. The reason why Al<sub>3</sub>Ni<sub>5</sub> cannot be found in Ref. [43] may be that the annealing temperature was too low to reach equilibrium in 500 h. According to the Al–Ca [35] and Ca–Ni

[40] binary phase diagrams, Al<sub>14</sub>Ca<sub>13</sub>, Al<sub>3</sub>Ca<sub>8</sub>, CaNi<sub>3</sub> and Ca<sub>2</sub>Ni<sub>7</sub> were present and stable at 773 K, while they were absent in the results of Ref. [43]. Apart from the published 773 K isothermal section, limited experimental data could be found in the literature. The shortage of experimental information affects the reliability of thermodynamic modelling and the design of alloys. Therefore, it is important to provide more experimental phase diagrams to improve the thermodynamic parameters in CALPHAD modelling for more reliable predictions. The present work comprises a study of the isothermal sections at 873 and 673 K with equilibrated alloys. The characterization of the phase transformations during DSC tests and the characterization of the primary crystallization phases in as-cast alloys were used to obtain the liquidus projection.

## Experimental procedure

The alloy samples with the nominal compositions listed in Table 2, 3 and 4 were prepared from Al<sub>45</sub>Ca<sub>43</sub>Ni<sub>12</sub> ternary master alloys (Hunan rare-earth metal research institute), nickel powder (99.99 wt%, China New Metal Materials Technology Co., Ltd) and

**Figure 2** **a** The 773 K isothermal section of the Al–Ca–Ni system determined experimentally by Manyako et al. [43] and **b** calculated isothermal section of Al–Ca–Ni system at 773 K.



aluminium rod (99.99 wt%, China New Metal Materials Technology Co., Ltd). Since the melting point of nickel is close to the boiling point of calcium, and the

metal activity of calcium is pretty strong, it was very important to avoid the use of pure Ca during alloy preparation.

**Table 2** Nominal compositions, primary crystallization phases of the Al–Ca–Ni alloys

Alloy no	Compositions (at.%)			Primary crystallization phases observed in as-cast alloys
	Al	Ca	Ni	
A1	85.56	10.23	4.21	$\tau_2$
A2	85.56	4.62	9.82	$\text{Al}_3\text{Ni}$
A3	76.33	6.24	17.44	$\text{Al}_3\text{Ni}_2$
A4	72.64	20.1	7.27	$\text{Al}_2\text{Ca}$

**Table 3** Constituent phases and compositions in the annealed Al–Ca–Ni alloys at 873 K

Alloy (no)	Composition (at.%)			Experimental results (at.%)			Phase determination
	Al	Ca	Ni	Al	Ca	Ni	
B1	85.56	10.23	4.21	82.51	8.53	8.96	$\tau_1$
				80.7	19.3	0	$\text{Al}_4\text{Ca}$
				100	0	0	Fcc_Al
B2	85.56	4.62	9.82	76.58	0	23.42	$\text{Al}_3\text{Ni}$
				81.77	8.87	9.36	$\tau_1$
				100	0	0	Fcc_Al
B3	78.17	11.72	10.11	79.7	20	0.3	$\text{Al}_4\text{Ca}$
				78.6	8.6	12.8	$\tau_3$
B4	76.33	6.24	17.44	75.75	0.11	24.14	$\text{Al}_3\text{Ni}$
				78.51	8.66	12.82	$\tau_3$
				81.62	8.53	9.85	$\tau_1$
B5	72.64	20.1	7.27	74.94	8.58	16.48	$\tau_2$
				66.16	33.52	0.33	$\text{Al}_2\text{Ca}$
				80.49	18.87	0.65	$\text{Al}_4\text{Ca}$
B6	70.1	3.55	26.36	63.58	0	36.42	$\text{Al}_3\text{Ni}_2$
				73.83	8.65	17.52	$\tau_2$
				76.76	0	23.24	$\text{Al}_3\text{Ni}$
B7	66.17	10.31	23.51	64.38	0	35.2	$\text{Al}_3\text{Ni}_2$
				74.49	8.61	16.9	$\tau_2$
				68.33	31.67	0	$\text{Al}_2\text{Ca}$
B8	60.64	9.68	29.68	63.73	0	36.27	$\text{Al}_3\text{Ni}_2$
				67.06	32.23	0.71	$\text{Al}_2\text{Ca}$
B9	55.33	24.35	20.32	49.82	0.58	49.54	AlNi
				66.34	33.21	0.45	$\text{Al}_2\text{Ca}$
				52.21	47.53	0.26	$\text{Al}_{14}\text{Ca}_{13}$
B10	45	43	12	49.67	0.74	49.59	AlNi
				51.93	47.76	0.31	$\text{Al}_{14}\text{Ca}_{13}$
				37.63	62.18	0.19	Liquid

An analytical balance with an error of about  $\pm 0.005$  g was used, and the weight of each sample was 5 g. In this work, a new method of alloy preparation was used as illustrated in Fig. 3 due to the specific properties of the Al–Ca–Ni ternary system. To avoid a reaction between the Ca and quartz tube, the alloy samples were melted in a corundum crucible which was pressed with tantalum foil into the quartz tube. Considering the difference of the thermal expansion coefficient between corundum and

quartz, a gap was left between the quartz tube and corundum crucible, as well as a quartz rod which was placed at the bottom of the quartz tube to avoid the rupture of quartz tube during cooling process.

The melting process was crucial during the alloy preparation due to the higher vapour pressure and extremely strong metal activity of calcium. The pressure of the argon atmosphere in the melting process would increase as the amount of calcium goes up. According to the properties of the raw



**Table 4** Constituent phases and compositions in the annealed Al–Ca–Ni alloys at 673 K

Alloy (no)	Composition (at.%)			Experimental results (at.%)			Phase determination
	Al	Ca	Ni	Al	Ca	Ni	
C1	85.56	10.23	4.21	81.47	9.34	9.18	$\tau_1$
				80.1	19.82	0.07	Al <sub>4</sub> Ca
				99.9	0.03	0.06	Fcc_Al
C2	85.56	4.62	9.82	74.32	0.04	25.63	Al <sub>3</sub> Ni
				80.57	9.28	10.14	$\tau_1$
				99.5	0.1	0.38	Fcc_Al
C3	78.17	11.72	10.11	80.4	18.98	0.62	Al <sub>4</sub> Ca
				78.51	8.88	12.61	$\tau_3$
C4	76.33	6.24	17.44	75.8	0	24.2	Al <sub>3</sub> Ni
				79.1	8.5	12.4	$\tau_3$
				80.8	8.7	10.5	$\tau_1$
C5	72.64	20.1	7.27	66.7	33.2	0.1	Al <sub>2</sub> Ca
				79.7	19.7	0.6	Al <sub>4</sub> Ca
				73.6	17.7	8.8	$\tau_2$
C6	70.1	3.55	26.36	62.68	0.24	37.08	Al <sub>3</sub> Ni <sub>2</sub>
				73.61	8.75	17.64	$\tau_2$
				76.4	0.17	23.43	Al <sub>3</sub> Ni
C7	66.17	10.31	23.51	62.89	0.25	36.86	Al <sub>3</sub> Ni <sub>2</sub>
				74.26	8.63	17.11	$\tau_2$
				66.14	33.08	0.78	Al <sub>2</sub> Ca
C8	60.64	9.68	29.68	61.69	0.2	38.11	Al <sub>3</sub> Ni <sub>2</sub>
				66.37	32.94	0.69	Al <sub>2</sub> Ca
C9	57.64	12.38	29.98	66.17	33.18	0.75	Al <sub>2</sub> Ca
				50.02	0.19	49.79	AlNi
C10	55.33	24.35	20.32	49.82	0.35	49.83	AlNi
				66.34	33.21	0.45	Al <sub>2</sub> Ca
				52.21	47.53	0.26	Al <sub>14</sub> Ca <sub>13</sub>
C11	45	43	12	49.82	0.4	49.78	AlNi
				26.74	72.97	0.31	Al <sub>3</sub> Ca <sub>8</sub>
				51.62	47.92	0.46	Al <sub>14</sub> Ca <sub>13</sub>
C12	36.8	35.2	28	49.82	0.35	49.83	AlNi
				27.48	0.66	71.86	Al <sub>3</sub> Ca <sub>8</sub>
				0.68	98.76	0.56	Fcc_Ca

materials, the samples were melted at 1200 °C for 1.5 h. Staying at high temperature for too long, serious volatilization of calcium could occur. Therefore, the cooling rates are 400 °C/h at 1000–1200 °C and 200 °C/h at 800–1000 °C, respectively. Quenching just below the liquidus temperature was appropriate, while looseness and shrinkage cavities could be formed at high temperature. Therefore, the samples were heated at 800 °C for 2 h then quenched. The argon pressure in the quartz tube, the melting time and temperature are the vital parameters in alloy preparation. As shown in Fig. 3, the silica capsule filled with raw materials was put into the furnace at

point A. After shaking, the melt was quenched at point B (Fig. 4).

Each of the samples produced was determined to be homogeneous and was then cut into pieces of the same size for different experiments. One piece was used to investigate the as-cast microstructure, and two of them were sealed in an evacuated, argon-filled quartz tube (0.6 atm) and annealed at 873 K for 60 days and 673 K for 150 days, respectively. To obtain equilibrated alloys, the samples should be annealed for a long time, especially at low temperature. After annealing, the alloys were taken out and quenched into cold water.

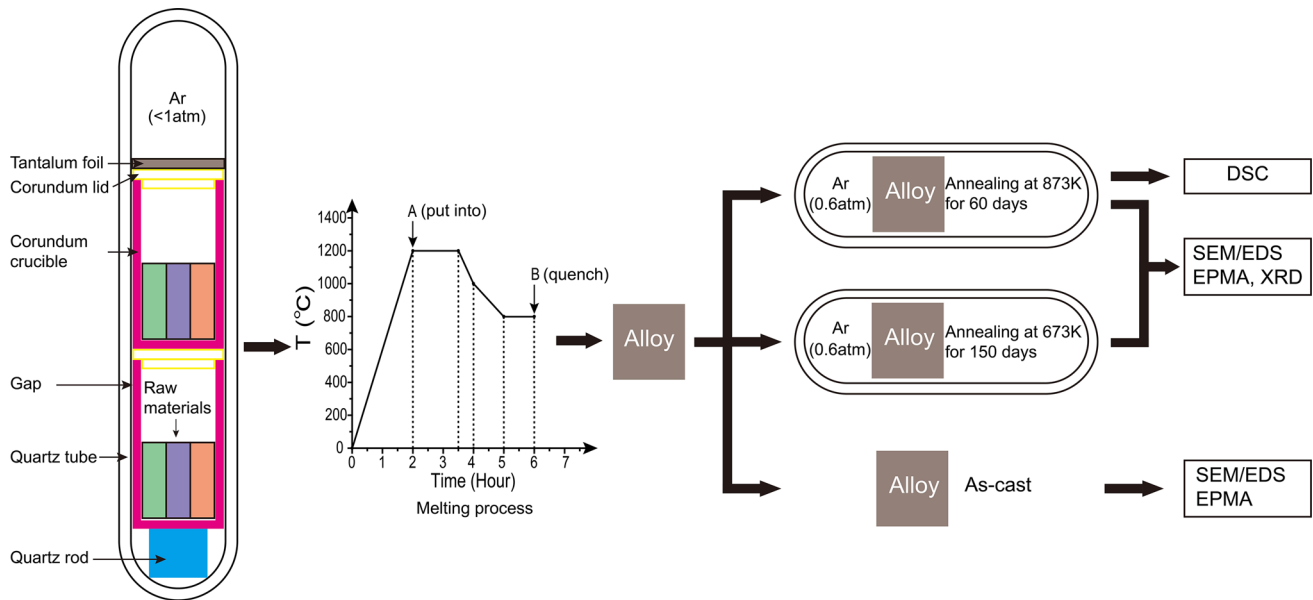


**Figure 3** The method of alloy preparation, melting process, heat treatment procedure and microstructure characterization methods.

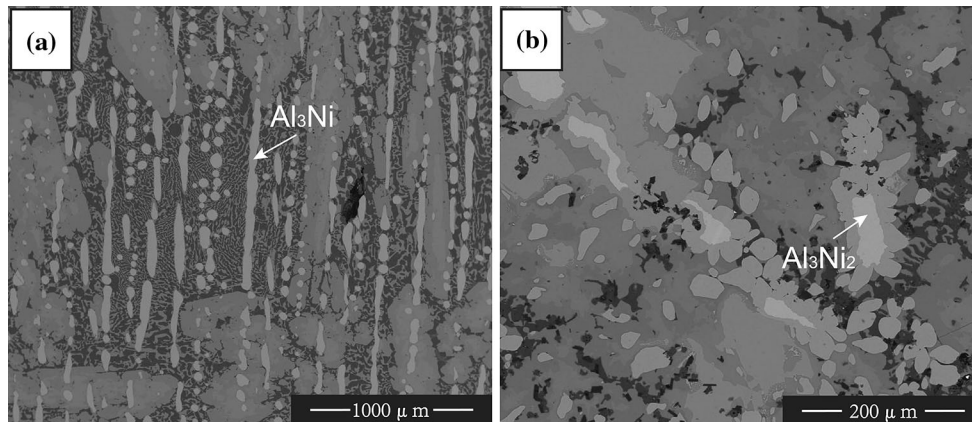


**Figure 4** BSE images of as-cast samples with the primary crystallization phases **a** sample A2 and **b** sample A3.

The samples were mounted, ground and polished according to standard metallographic practices. The microstructures, compositions and constituent phases of the annealed samples were determined by SEM (FEI Quanta 200), EPMA (JEOL JXA-8230) with a 15 kV voltage and 10 mA current, DSC (NETZSCH STA 449C, corundum crucible, argon protected) with a heating rate of 10 K/min, and XRD was also performed using a Cu  $K\alpha$  radiation source on a Rigaku D-max/2550 VB + X-ray diffractometer at 40 kV/250 mA with a scanning range of about 10–90° and scan speed of about 8°/min.

## Thermodynamic models

### Solution phases

The substitutional solution model is adopted to describe all the solution phases, i.e. liquid, Fcc, Bcc and Hcp. The molar Gibbs energy can be expressed as follows:

$$G_m^\varphi = \sum_{i=\text{Al,Ca,Ni}} x_i^0 G_i^\varphi + RT \sum_{i=\text{Al,Ca,Ni}} x_i \ln(x_i) + {}^{\text{ex}}G_m^\varphi \quad (1)$$

where  $x_i$  is mole fraction of component  $i$  ( $i = \text{Al, Ca, Ni}$ ),  ${}^0G_i^\varphi$  is the molar Gibbs energy of the pure



element  $i$  with the structure  $\varphi$  phase, which is taken from the Scientific Group Thermodata Europe (SGTE) Pure Elements Database [49],  $R$  is the gas constant,  $T$  is the temperature in kelvin and  ${}^{\text{ex}}G_m^\varphi$  is the excess Gibbs energy formulated with the Redlich–Kister polynomial [50]:

$$\begin{aligned}
 {}^{\text{ex}}G^\varphi = & x_{\text{Al}}x_{\text{Ca}} \sum_{j=0,1,\dots}^n (x_{\text{Al}} - x_{\text{Ca}})^{j(j)} L_{\text{Al,Ca}}^\varphi + x_{\text{Al}}x_{\text{Ni}} \\
 & \sum_{j=0,1,\dots}^n (x_{\text{Al}} - x_{\text{Ni}})^{j(j)} L_{\text{Al,Ni}}^\varphi + x_{\text{Ca}}x_{\text{Ni}} \\
 & \sum_{j=0,1,\dots}^n (x_{\text{Ca}} - x_{\text{Ni}})^{j(j)} L_{\text{Ca,Ni}}^\varphi + x_{\text{Al}}x_{\text{Ca}}x_{\text{Ni}} \\
 & \left( x_{\text{Al}}^{(0)} L_{\text{Al,Ca,Ni}}^\varphi + x_{\text{Ca}}^{(1)} L_{\text{Al,Ca,Ni}}^\varphi + x_{\text{Ni}}^{(2)} L_{\text{Al,Ca,Ni}}^\varphi \right) \quad (2)
 \end{aligned}$$

where  ${}^jL_{\text{Al,Ni}}^\varphi$ ,  ${}^jL_{\text{Al,Ca}}^\varphi$  and  ${}^jL_{\text{Ca,Ni}}^\varphi$  are the interaction parameters between elements Al and Ni, Al and Ca, and Ca and Ni, respectively. These parameters are cited from Dupin et al. [26], Ozturk et al. [35] and Uremovich et al. [40], separately.  $L_{\text{Al,Ca,Ni}}^\varphi$  is the ternary interaction parameter between Al, Ca and Ni.

The general form of the interaction parameters of  ${}^kL_{\text{Al,Ni,Ca}}^\varphi$  ( $k = 0, 1, 2$ ) is shown as follows:

$${}^kL_{\text{Al,Ni,Ca}}^\varphi = A_k + B_k T \quad (3)$$

where  $A_k$  and  $B_k$  are the constant to be optimized in this present work. As for the ternary interaction parameters, only  ${}^kL_{\text{Al,Ni,Ca}}^{\text{liquid}}$  was evaluated for liquid in this work.

There was no ternary solubility in the binary intermetallic phases. All binary parameters are cited from the literature.

### Ternary intermetallic phases

In the Al–Ca–Ni ternary system,  $\tau_1$ ,  $\tau_2$  and  $\tau_3$  were modelled as the stoichiometric phase  $\text{Al}_x\text{Ca}_y\text{Ni}_z$ . The Gibbs energy can be expressed as:

$$\begin{aligned}
 G_{\text{Al:Ca:Ni}} = & C + DT + \frac{x}{x + y + z} {}^0G_{\text{Al}}^{\text{HSER}} \\
 & + \frac{y}{x + y + z} {}^0G_{\text{Ca}}^{\text{HSER}} + \frac{z}{x + y + z} {}^0G_{\text{Ni}}^{\text{HSER}} \quad (4)
 \end{aligned}$$

where  $C$  and  $D$  are the parameters to be optimized in this work.  ${}^0G_{\text{Al}}^{\text{HSER}}$ ,  ${}^0G_{\text{Ca}}^{\text{HSER}}$  and  ${}^0G_{\text{Ni}}^{\text{HSER}}$  are the molar Gibbs energy of the pure element Al, Ca and Ni with stable structure, which are cited from the SGTE [49].

## Results and discussion

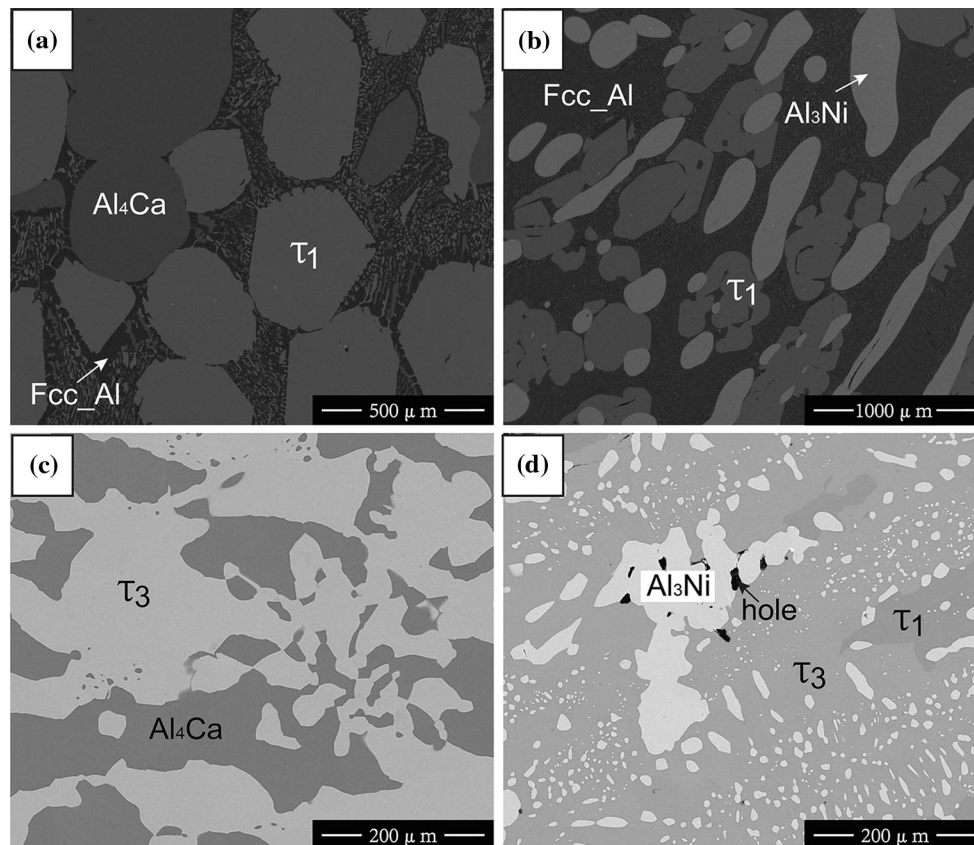
### Experimental aspects

Constituent phases in some representative as-cast alloys A1, A2, A3, A4 are determined based on EPMA and XRD technology. The BSE images of as-cast alloy samples are presented in Fig. 3. Table 2 summarizes the primary crystallization phases observed in the as-cast alloys. As shown in Fig. 3, the bright phase with a strip shape ( $\text{Al}_3\text{Ni}$ ) in sample A2 and the inside bright phase ( $\text{Al}_3\text{Ni}_2$ ) in sample A3 have been identified as the primary phases, respectively.

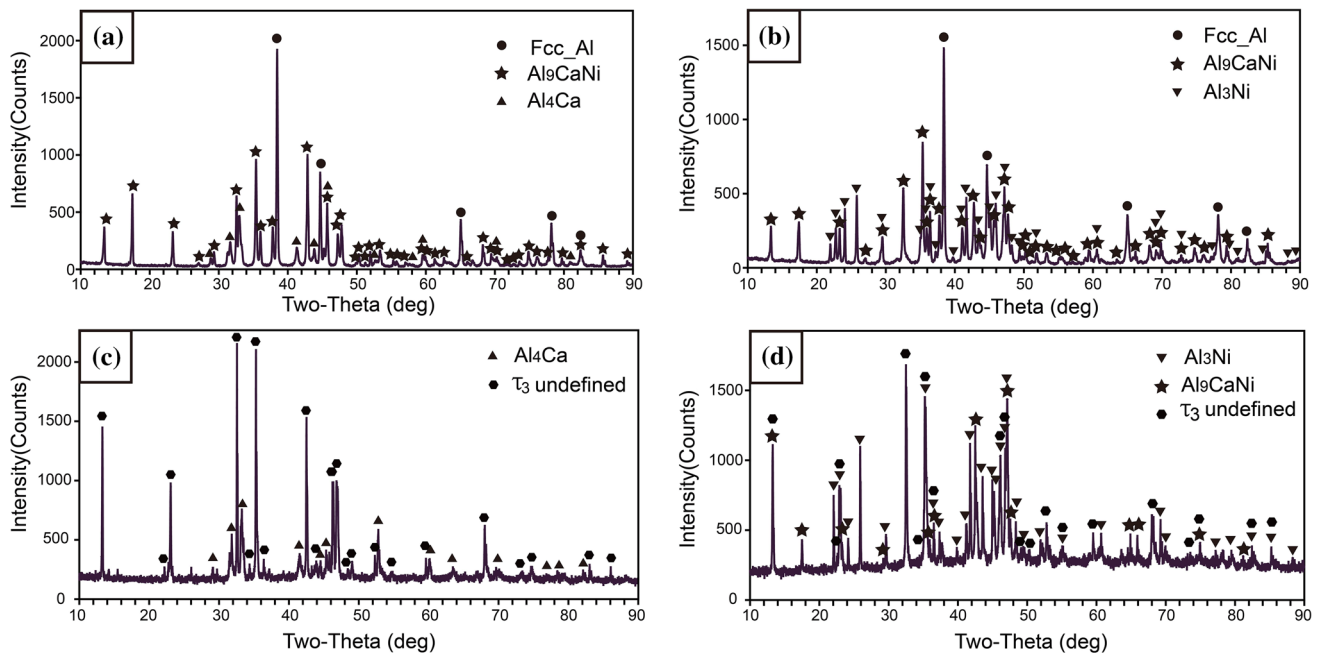
Phase equilibria of the Al–Ca–Ni ternary system at 873 K were studied on the basis of experimental results in this work. We found that although the number of phases was less than three and the composition of each phase was homogenized, which means an equilibrium state has been reached, some solidification morphology still remains due to the low interface mobility. The constituent phases in the annealed alloys are summarized in Table 3 and were identified by a combination of XRD, SEM and EPMA.

Figure 5 presents the BSE images of annealed Al-rich samples B1, B2, B3 and B4. In sample B1, a three-phase equilibrium between black Fcc\_Al, dark grey  $\text{Al}_4\text{Ca}$  and light grey  $\tau_1$  was observed (Fig. 5a). In sample B1, as shown in Fig. 5b, the black areas correspond to the Fcc\_Al phase; the bright areas stand for the  $\text{Al}_3\text{Ni}$  phase, and the light-grey areas represent the  $\tau_1$  phase. Figure 5c exhibits the BSE of sample B3, and two phases  $\text{Al}_4\text{Ca}$  and  $\tau_3$  are observed. Figure 5d illustrates the BSE image of sample B4 which clearly contains three phases, dark grey  $\tau_1$ , light grey  $\tau_3$  and bright  $\text{Al}_3\text{Ni}$ . The XRD patterns of these samples are illustrated in Fig. 6.

In this present work, a new compound  $\tau_3$  was detected with the formula identified as  $\text{Al}_{78}\text{Ca}_9\text{Ni}_{13}$ . This is based on EPMA data only. Considering the chemical component of  $\tau_3$  was close to  $\tau_1$  and  $\tau_2$ , the XRD and BSE analysis were used to distinguish  $\tau_3$  from  $\tau_1$  and  $\tau_2$ . In order to improve accuracy of the crystallographic data of  $\tau_3$ , the XRD patterns of sample B3 (only contain  $\text{Al}_4\text{Ca}$  and  $\tau_3$ ) were used to analyse it. As shown in Fig. 7, significant differences in the main diffraction peaks at specific angles could be observed between  $\tau_2$  and  $\tau_3$ , such as  $2\theta = 22.1, 36.2, 43.8, 44.2$  and  $45.6$ . As is illustrated in Fig. 8,



**Figure 5** BSE images of sample **a** B1, **b** B2, **c** B3 and **d** B4 annealed at 873 K for 60 days.



**Figure 6** XRD patterns of **a** sample B1, **b** sample B2, **c** sample B3 and **d** sample B4 annealed at 873 K for 60 days.

**Figure 7** XRD pattern of sample B3 and the diffraction peak of  $\text{Al}_9\text{CaNi}$ ,  $\text{Al}_8\text{CaNi}_2$  and  $\text{Al}_4\text{Ca}$  are labelled.

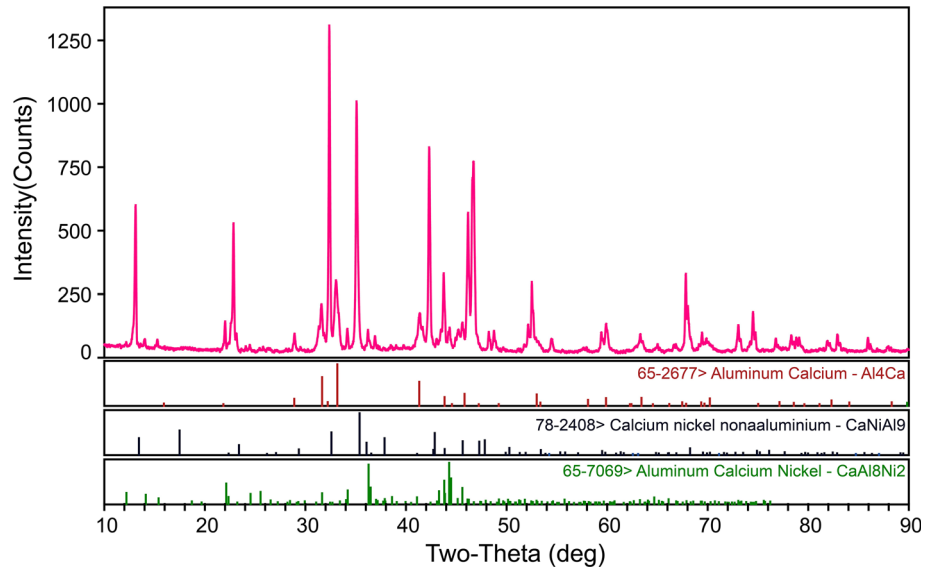


**Figure 8** The line scan between  $\tau_1$  and  $\tau_3$  in annealed sample B4.

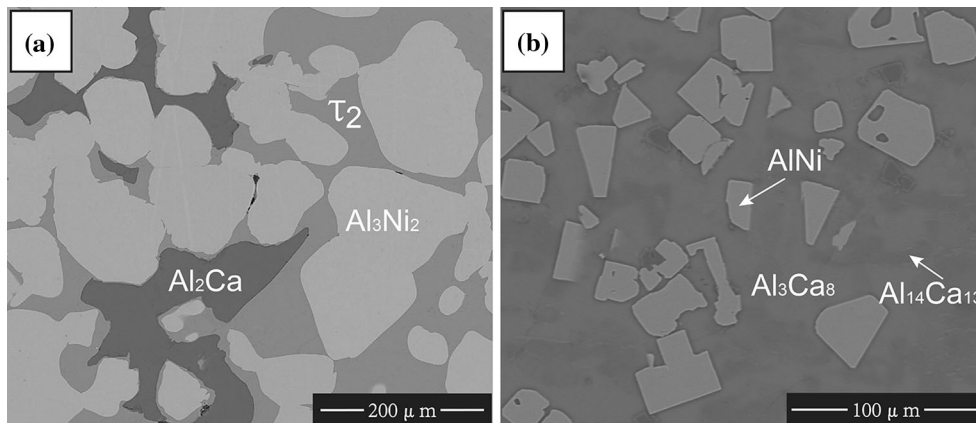
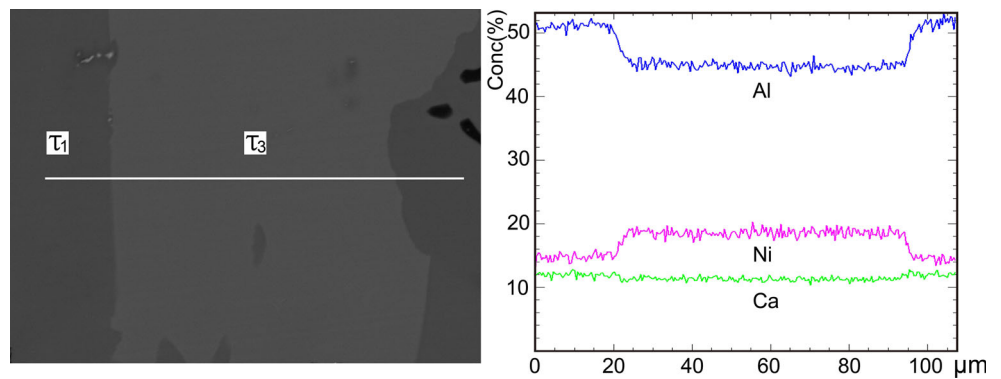
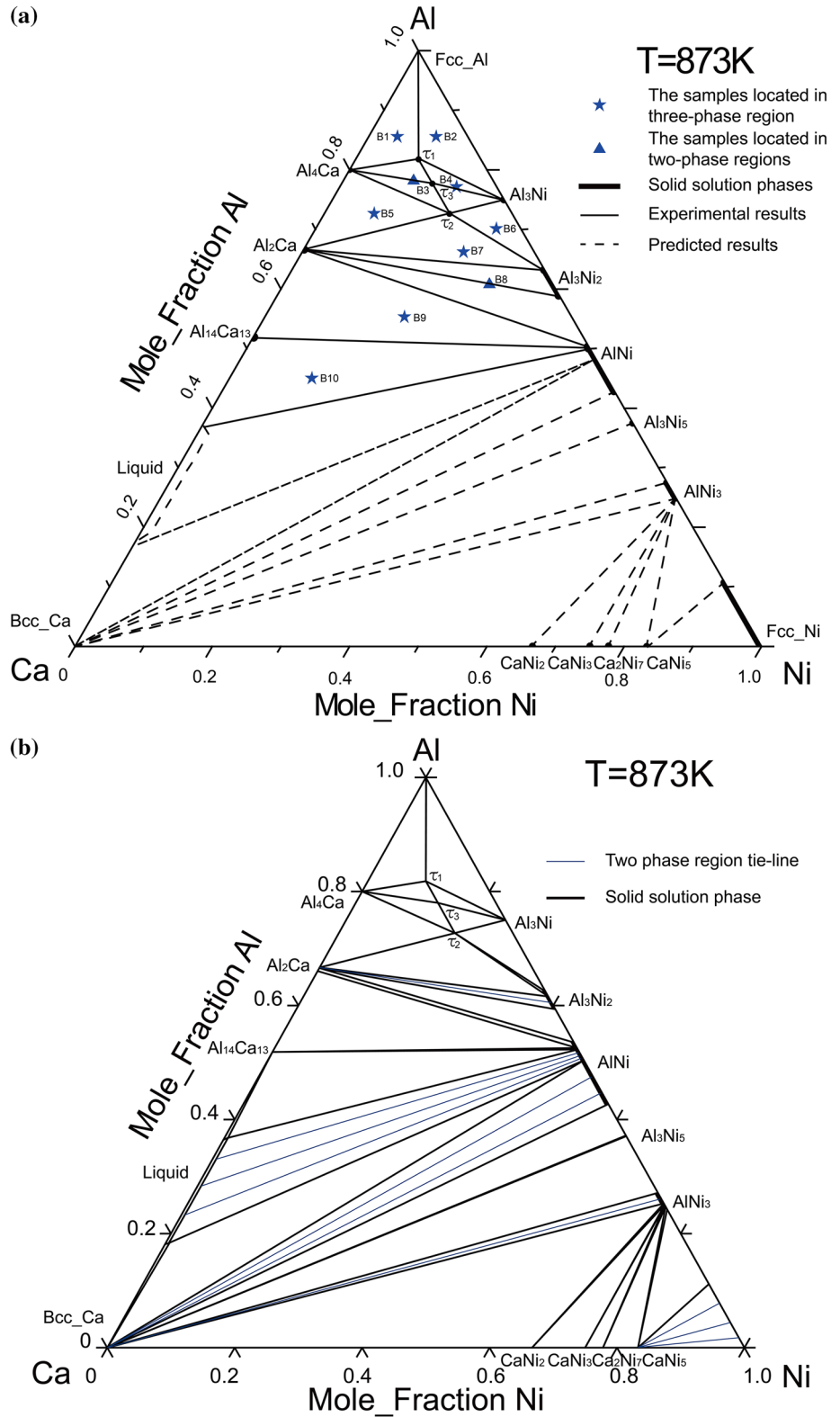


**Figure 9** BSE images of sample **a** C7 and **b** C11 annealed at 673 K for 150 days.

obvious phase boundaries between  $\tau_3$  and  $\tau_1$  could be found in the BSE image of the line scan in sample B4, and a change of composition was also determined by EPMA. Comparing the diffraction peaks of  $\tau_1$ , the

diffraction peaks at  $2\theta = 17.2, 36, 38$  and  $45.6$  are absent. The diffraction peaks at  $2\theta = 13.2, 23.2, 32.5, 35.4$  and  $42.8$  have changed position unpredictably. Therefore, we judged that  $\tau_3$  is an individual

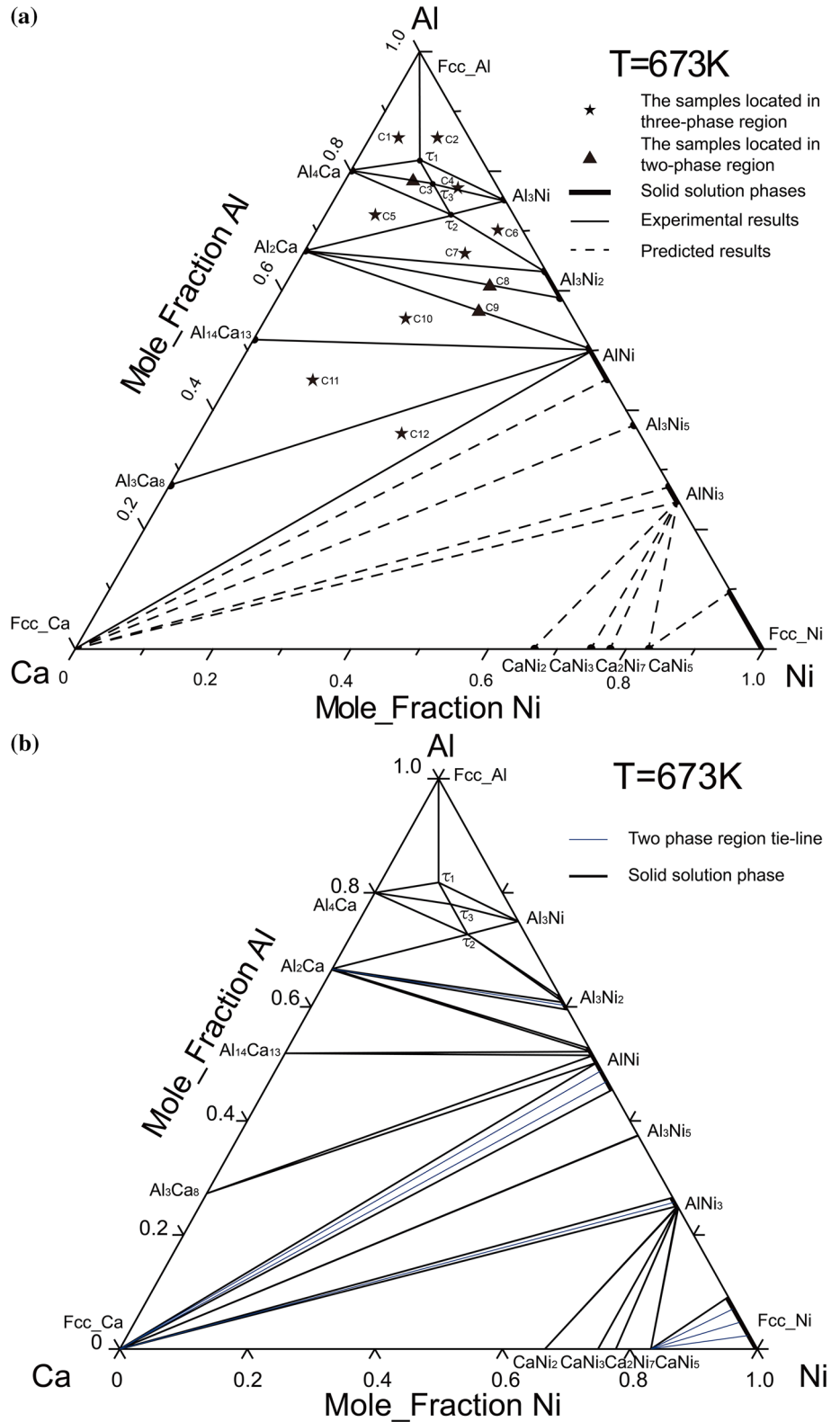
**Figure 10** **a** Experimentally determined 873 K isothermal section of Al–Ca–Ni system and **b** calculated isothermal section of Al–Ca–Ni system at 873 K.



compound rather than the solution phase of  $\tau_1$  or  $\tau_2$  and that more accurate defining of the compound's crystal structure requires further investigation.

Phase relations in the Al–Ca–Ni system at 673 K were also obtained based on the experimental information in this work. After heat treatment for

**Figure 11** **a** Experimentally determined 673 K isothermal section of Al–Ca–Ni system and **b** calculated isothermal section of Al–Ca–Ni system at 673 K.





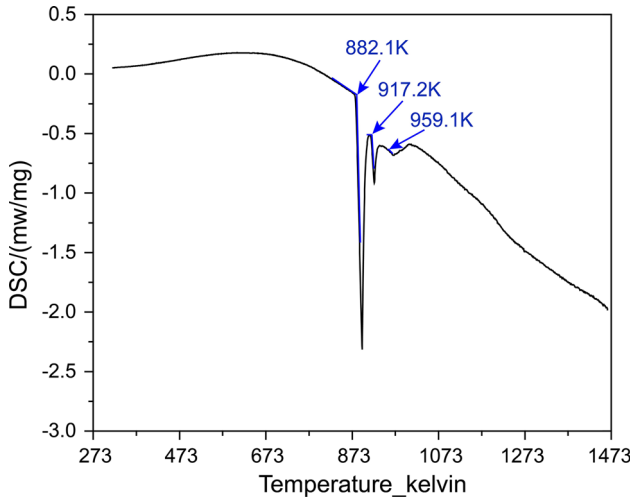


**Figure 12** DSC curve of annealed sample B1.

150 days, some solidification morphology still remains, due to low interface mobility. However, the composition of each phase was homogenized, which means an equilibrium state had been reached. Table 4 summarizes the nominal compositions of the alloys and the phases in equilibrium which were identified by a combination of XRD, SEM and EPMA. All the phases can be easily differentiated based on their brightness on greyscale images and chemical

composition. Microstructures in backscattered electrons (BSE) of C7 and C11 are shown in Fig. 9.

The phase relations at 673 K were similar to those at 873 K, but with slight differences in the phase composition.  $Al_3Ca_8$  could stably exist at 673 K, while it was absent at 873 K. The three-phase equilibrium of  $Al_{14}Ca_{13} + AlNi + Al_3Ca_8$  at 673 K and  $Al_{14}Ca_{13} + AlNi + liquid$  at 873 K was determined, respectively. Based on the experimental results obtained in this work and pertinent information from relevant binary systems published in the literature, the isothermal section of the Al–Ca–Ni ternary system at 873 and 673 K was constructed and is shown in Figs. 10a and 11a. In comparison with the 773 K isothermal section reported by Ref [43], a new ternary phase  $\tau_3$  was detected based on XRD and EPMA. Two additional binary phases,  $Al_{14}Ca_{13}$  and  $Al_3Ca_8$ , were also determined. The composition regions of  $Al_3Ni_2$  were 38.48–40.96 at.% Ni at 673 K and 37.51–41.17 at.% Ni at 873 K, respectively. The  $Al_3Ni_2$  phase was treated as stoichiometric phases in the result of Ref. [43]. In Tables 3 and 4, it could be found that only very small or even negligible ternary solubility in the binary intermetallics could be found experimentally. Based on DSC analysis of sample B1 (Fig. 12), the ternary eutectic reaction

**Table 5** Comparison of the optimized standard enthalpies of formation with results from first-principles calculations

Phase	Structure	First-principles calculations (J/mol)	CALPHAD (J/mol)
$\tau_1$	$Al_9CaNi$ , hP22	−25889	−27002.4
$\tau_2$	$Al_8Fe_2Ce$ , oP44	−40156	−45097.2

**Table 6** Thermodynamics parameters of Al–Ca–Ni ternary system in this work

Phase	Thermodynamic parameters	Ref
Liquid	(Al, Ca, Ni)	
	${}^0L_{Al,Ca,Ni}^{Liquid} = 5545 + 12.368 * T$	This work
	${}^1L_{Al,Ca,Ni}^{Liquid} = -21847 + 11.769 * T$	This work
	${}^2L_{Al,Ca,Ni}^{Liquid} = 4780 + 5.03 * T$	This work
$\tau_1$	(Al) <sub>0.818</sub> (Ca) <sub>0.091</sub> (Ni) <sub>0.091</sub> ${}^0G_{Al:Ca:Ni}^{\tau_1} = -27002.4 + 6.1 * T + 0.818{}^0G_{Al}^{HSER} + 0.091{}^0G_{Ca}^{HSER} + 0.091{}^0G_{Ni}^{HSER}$	This work
$\tau_2$	(Al) <sub>0.727</sub> (Ca) <sub>0.091</sub> (Ni) <sub>0.182</sub> ${}^0G_{Al:Ca:Ni}^{\tau_2} = -45097.2 + 11.4 * T + 0.727{}^0G_{Al}^{HSER} + 0.091{}^0G_{Ca}^{HSER} + 0.182{}^0G_{Ni}^{HSER}$	This work
$\tau_3$	(Al) <sub>0.78</sub> (Ca) <sub>0.091</sub> (Ni) <sub>0.129</sub> ${}^0G_{Al:Ca:Ni}^{\tau_3} = -34399.4225 + 8.05 * T + 0.78{}^0G_{Al}^{HSER} + 0.091{}^0G_{Ca}^{HSER} + 0.129{}^0G_{Ni}^{HSER}$	This work

${}^0G_{Al}^{HSER}$ ,  ${}^0G_{Ca}^{HSER}$  and  ${}^0G_{Ni}^{HSER}$  cited from the SGTE [48]



**Figure 13** Calculated liquidus projection of the Al–Ca–Ni system together with the primary crystallization phases observed in the as-cast samples.

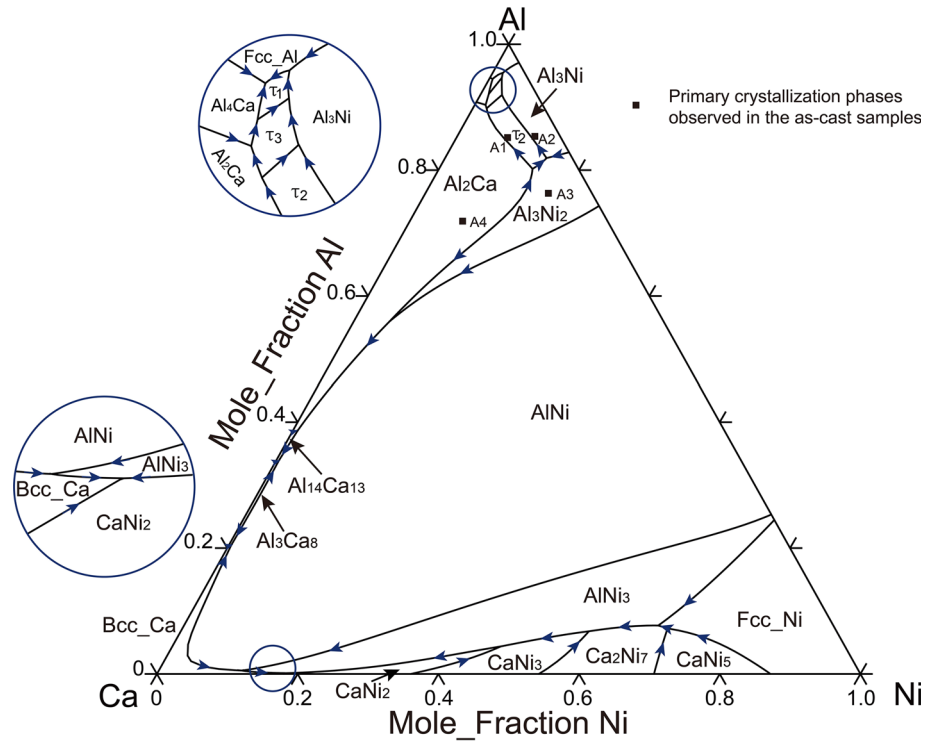


**Table 7** The calculated invariant reactions and their temperatures of the Al–Ca–Ni system

Type	Reaction	Calculated T/K	Experimental T/k
U <sub>1</sub>	Liquid + CaNi <sub>5</sub> → Ca <sub>2</sub> Ni <sub>7</sub> + Fcc_Ni	1288.7	–
U <sub>2</sub>	Liquid + Fcc_Ni → AlNi <sub>3</sub> + Ca <sub>2</sub> Ni <sub>7</sub>	1270.5	–
U <sub>3</sub>	Liquid + Ca <sub>2</sub> Ni <sub>7</sub> → AlNi <sub>3</sub> + CaNi <sub>3</sub>	1180.6	–
P <sub>1</sub>	Liquid + Al <sub>3</sub> Ni <sub>2</sub> + Al <sub>2</sub> Ca → τ <sub>2</sub>	1130.2	–
U <sub>4</sub>	Liquid + Al <sub>3</sub> Ni <sub>2</sub> → τ <sub>2</sub> + Al <sub>3</sub> Ni	1111.0	–
U <sub>5</sub>	Liquid + CaNi <sub>3</sub> → AlNi <sub>3</sub> + CaNi <sub>2</sub>	1094.4	–
P <sub>2</sub>	Liquid + Al <sub>2</sub> Ca + τ <sub>2</sub> → τ <sub>3</sub>	978.7	979
U <sub>6</sub>	Liquid + AlNi → Bcc_Ca + AlNi <sub>3</sub>	971.0	–
U <sub>7</sub>	Liquid + τ <sub>2</sub> → τ <sub>3</sub> + Al <sub>3</sub> Ni	965.3	959
U <sub>8</sub>	Liquid + Al <sub>2</sub> Ca → τ <sub>3</sub> + Al <sub>4</sub> Ca	964.5	–
U <sub>9</sub>	Liquid + Al <sub>3</sub> Ni <sub>2</sub> → Al <sub>2</sub> Ca + AlNi	950.1	–
P <sub>3</sub>	Liquid + Al <sub>4</sub> Ca + τ <sub>3</sub> → τ <sub>1</sub>	934.0	–
U <sub>10</sub>	Liquid + τ <sub>3</sub> → Al <sub>3</sub> Ni + τ <sub>1</sub>	909.7	–
E <sub>1</sub>	Liquid → Bcc_Ca + AlNi <sub>3</sub> + CaNi <sub>2</sub>	899.0	–
U <sub>11</sub>	Liquid + Al <sub>2</sub> Ca → AlNi + Al <sub>14</sub> Ca <sub>13</sub>	898.4	–
U <sub>12</sub>	Liquid + Al <sub>3</sub> Ni → Fcc_Al + τ <sub>1</sub>	894.1	–
E <sub>2</sub>	Liquid → Fcc_Al + τ <sub>1</sub> + Al <sub>4</sub> Ca	881.8	882.1
E <sub>3</sub>	Liquid → AlNi + Al <sub>14</sub> Ca <sub>13</sub> + Al <sub>3</sub> Ca <sub>8</sub>	826.2	–
E <sub>4</sub>	Liquid → AlNi + Al <sub>3</sub> Ca <sub>8</sub> + Bcc_Ca	826.1	–

U, quasi-peritectic reaction; P, peritectic reaction; E, eutectic reaction

(L  $\rightarrow$  Al + Al<sub>4</sub>Ca + Al<sub>9</sub>CaNi) was clarified to take place at 882.1 K.

### Calculated aspects

The first-principle calculations were employed to calculate the enthalpies of formation of the ternary compounds in this system. First-principle calculations were performed by using the scalar relativistic all-electron Blöchl's projector augmented-wave (PAW) method [51, 52] within the generalized gradient approximation (GGA), as implemented in the highly efficient Vienna ab initio simulation package (VASP) [53, 54]. For the GGA exchange–correlation function, Perdew–Bucke–Ernzerhof parameterisation (PBE) [55, 56] was employed. A plane-wave energy cut-off of 404 eV was held constant for the study of the different Al<sub>x</sub>Ca<sub>y</sub>Ni<sub>z</sub> compounds. Brillouin zone integrations were performed using Monkhorst and Pack [57] K-point meshes, and the Methfessel and Paxton [58] technique with a smearing parameter of 0.2 eV. The reciprocal space (*k*-point) meshes were increased to achieve convergence to a precision of 1 meV/atom. The total energy was converged numerically to less than  $1 \times 10^{-6}$  eV/U with respect to electronic, ionic and unit cell degrees of freedom, and the latter two parameters were relaxed using calculated forces with a preconditioned conjugated gradient algorithm. The calculated formation enthalpies from first-principle calculations are shown in Table 5.

On the basis of lattice stabilities cited from Dinsdale [49], the optimization work was performed by the parrot module in the Thermo-Calc program developed by Sundman et al. [59]. The Pandat program [60] was applied to check the database. The thermodynamic parameters of the ternary compounds were assessed next by using phase diagram data and the standard enthalpies of formation, which were calculated from first-principle calculations. The parameters for the liquid phase were optimized using invariant reaction temperatures measured with DSC and the primary crystallization information from the experimental results. All the parameters were finally evaluated together to give a reasonable description of this system. The optimized parameters are listed in Table 6.

The calculated isothermal sections at 873, 773 and 673 K are shown in Figs. 10b, 2b and 11b. In comparison with the experimental isothermal section, the calculated phase relationships were in good agreement with the experimental results.

With the optimized thermodynamic parameters for the Al–Ca–Ni system, the liquidus projection was calculated as displayed in Fig. 13. The calculated primary crystallization phases are labelled in Fig. 13, and the observed primary crystallization phases in as-cast samples are summarized in Table 2. Good fit was found between the calculated results and the experimental observations from the as-cast samples.

An enlarged portion is also shown in Fig. 13 in order to present the ternary invariant reactions in the Al-rich corner clearly. The calculated invariant reactions and their temperatures of the Al–Ca–Ni ternary system are listed in Table 7. For comparison, the experimental phase transition temperatures are given as well, and these were determined from DSC analysis. The differences between the calculated and measured temperatures of invariant reactions were all within error.

### Conclusions

By using equilibrated alloys, the isothermal section of the Al–Ca–Ni ternary system at 873 and 673 K has been critically studied using SEM, EPMA and XRD. A new ternary phase  $\tau_3$  was first detected and confirmed to exist, and the binary intermetallic phases Al<sub>14</sub>Ca<sub>13</sub> (in both 873 and 673 K) and Al<sub>3</sub>Ca<sub>8</sub> (673 K) were also determined. All present sample compositions are Al-rich: A1–A4 samples >72.64 at.% Al, B1–B10, C1–C11 >45 at.% Al, only C12 at 36.8 at.% Al. The primary crystallization phases in as-cast alloys have been observed and used as reference information on the calculated liquidus surface. Based on the experimental results of this work and the published literature, the Al–Ca–Ni ternary system has been assessed by means of the CALPHAD approach and first-principle calculations. A generally satisfactory agreement was obtained between the calculated results and experimental data in the Al-rich region, proving the validity of present thermodynamic modelling techniques. The calculated data in the Al-poor region are a very plausible prediction, but not validated.

### Acknowledgements

The authors would like to express gratitude to the financial support of the National Key Technologies

Research and Development Program of China (Grant No. 2016YFB0701301) and the National Natural Science Foundation of China (Grant Nos. 51371200, 51671218 and 51501229). The authors also would like to give thanks to Mr. Carl Meggs (University of Birmingham) for the English improvement.

### Compliance with ethical standards

**Conflict of interest** The authors declare that they have no conflict of interest.

**Electronic supplementary material:** The online version of this article (doi:[10.1007/s10853-017-1338-5](https://doi.org/10.1007/s10853-017-1338-5)) contains supplementary material, which is available to authorized users.

### References

- [1] Inoue A, Shen B, Koshiba H, Kato H, Yavari AR (2003) Cobalt-based bulk glassy alloy with ultra-high strength and soft magnetic properties. *Nat Mater* 2:661–663
- [2] Schroers J, Johnson WL (2004) Ductile bulk metallic glass. *Phys Rev Lett* 93:255506
- [3] Zhang B, Pan MX, Zhao DQ, Wang WH (2004) “Soft” bulk metallic glasses based on cerium. *Appl Phys Lett* 85:61–63
- [4] Liu YH, Wang G, Wang RJ, Zhao DQ, Pan MX, Wang WH (2007) Super plastic bulk metallic glasses at room temperature. *Science* 315:1385–1388
- [5] Lindsay Greer A (2015) New horizons for glass formation and stability. *Nat Mater* 14:542–546
- [6] Guo S, Liu Y (2012) Estimation of critical cooling rates for formation of amorphous alloys from critical sizes. *J Noncryst Solids* 358:2753–2758
- [7] Ge L, Hui X, Wang ER, Chen GL, Arroyave R, Liu ZK (2008) Prediction of the glass forming ability in Cu–Zr binary and Cu–Zr–Ti ternary alloys. *Intermetallics* 16:27–33
- [8] Wang JQ, Liu YH, Imhoff S, Chen N, Louzguine-Luzgin DV, Takeuchi A, Chen MW, Kato H, Perepezko JH, Inoue A (2012) Enhance the thermal stability and glass forming ability of Al-based metallic glass by Ca minor-alloying. *Intermetallics* 29:35–40
- [9] Ayers JD, Jones HN, Vold CL (1993) Stabilization of aluminum and magnesium base metallic glasses by the addition of calcium. *Scr Metall Mater* 29:205–209
- [10] Han FF, Inoue A, Han Y, Kong FL, Zhu SL, Shalaan E, Al-Marzouki F (2016) High formability of glass plus fcc-Al phases in rapidly solidified Al-based multicomponent alloy. *J Mater Sci* 52:1246–1254. doi:[10.1007/s10853-016-0394-6](https://doi.org/10.1007/s10853-016-0394-6)
- [11] Jiang YR, Li X, Jiang Y, Huang SH, Shi X, Mao C, Zhang LG, Liu LB, Zheng F (2017) Experimental investigation of phase relations in Al–Co–Y ternary system. *Calphad* 56:1–9
- [12] Li X, Liu LB, Jiang Y, Huang GX, Wang X, Jiang YR, Liang JS, Zhang LG, Shi X (2016) Thermodynamic evaluation of the phase equilibria and glass-forming ability of the Al–Co–Gd system. *Calphad* 52:57–65
- [13] Bao XH, Liu LB, Jiang YR, Jiang Y, Mao C, Li X, Zhang LG (2016) Thermodynamic assessment of the Al–Ba system. *J Phase Equilib Diffus* 37:345–349
- [14] Huang SX, Zhang XD, Jiang Y, Jiang YR, Mao C, Wu D, Liu LB, Zhang LG (2017) Experimental investigation of Ti–Nb–Co at 1000°C. *Mater Des* 115:170–178
- [15] Bo H, Liu LB, Hu JL, Jin ZP (2015) Experimental investigation and thermodynamic modeling of the Al–Dy–Zr system. *J Mater Sci* 50:6427–6436. doi:[10.1007/s10853-015-9197-4](https://doi.org/10.1007/s10853-015-9197-4)
- [16] Bai WM, Jiang Y, Guo ZY, Zeng LJ, Tan MY, Meggs C, Zhang LG, Liu LB, Jin ZP (2017) Experimental and thermodynamic investigation of Al–Cu–Nd ternary system. *Mater Chem Phys* 195:94–104
- [17] Kaufman L, Bernstein H (1970) Computer calculation of phase diagrams with special reference to refractory metals. Academic Press, New York
- [18] Alexander WO, Vaughan NB (1937) Investigation of phase equilibria in Al–Ni system. *J Inst Met* 61:247–260
- [19] Nash P, Singleton MF, Murray JL (1991) In: Nash P (ed) Phase diagrams of binary nickel alloys. ASM International, Materials Park, pp 3–11
- [20] Okamoto H (1993) Phase diagram updates: section III: Al–Ni. *J Phase Equilib* 14:257–259
- [21] Kaufman L, Nesor H (1978) Coupled phase diagrams and thermochemical data for transition metal binary systems—V. *Calphad* 2:325–348
- [22] Du Y, Clavaguera N (1996) Thermodynamic assessment of the Al–Ni system. *J Alloys Compd* 237:20–32
- [23] Ansara I, Dupin N, Lukas HL, Sundman B (1997) Thermodynamic assessment of the Al–Ni system. *J Alloys Compd* 247:20–30
- [24] Andersson JO, Guillermet AF, Hillert M, Jansson B, Sundman B (1986) A compound-energy model of ordering in a phase with sites of different coordination numbers. *Acta Metall* 34:437–445
- [25] Huang W, Chang YA (1998) A thermodynamic analysis of the Ni–Al system. *Intermetallics* 6:487–498
- [26] Dupin N, Ansara I, Sundman B (2001) Thermodynamic reassessment of the ternary system Al–Cr–Ni. *Calphad* 25:279–298
- [27] Zhang F, Chang YA, Du Y, Chen SL, Oates WA (2003) Application of the cluster-site approximation (CSA) model

- to the Fcc phase in the Ni–Al system. *Acta Mater* 51:207–216
- [28] Chen HL, Doernberg E, Svoboda P, Schmid-Fetzer R (2011) Thermodynamics of the Al<sub>3</sub>Ni phase and revision of the Al–Ni system. *Thermochim Acta* 512:189–195
- [29] Wang Y, Cacciamani G (2016) Thermodynamic modeling of the Al–Cr–Ni system over the entire composition and temperature range. *J Alloys Compd* 688:422–435
- [30] Hansen M, Anderko K (1958) *Constitution of binary alloys*, 2nd edn. McGraw-Hill, New York
- [31] Huang B, Corbett JD (1998) Two new binary calcium–aluminum compounds: Ca<sub>13</sub>Al<sub>14</sub>, with a novel two-dimensional aluminum network, and Ca<sub>8</sub>Al<sub>3</sub>, an Fe<sub>3</sub>Al-type analogue. *Inorg Chem* 37:5827–5833
- [32] Kevorkov D, Schmid-Fetzer R (2001) The Al–Ca system, Part 1: experimental investigation of phase equilibria and crystal structures. *Z. Metall* 92:946–952
- [33] Ozturk K, Chen LQ, Liu ZK (2002) Thermodynamic assessment of the Al–Ca binary system using random solution and associate models. *J Alloys Compd* 340:199–206
- [34] Wolverton C, Yan XY, Vijayaraghavan R, Ozolins V (2002) Incorporating first-principles energetics in computational thermodynamics approaches. *Acta Mater* 50:2187–2197
- [35] Ozturk K, Zhong Y, Chen LQ, Liu ZK, Sofu JO, Wolverton C (2005) Linking first-principles energetics to CALPHAD: an application to thermodynamic modeling of the Al–Ca binary system. *Metall Mater Trans A* 36:5–13
- [36] Takeuchi Y, Mochizuki K, Watanabe M, Obinata I (1966) The alloys of nickel with alkaline earth metals. *Metallurgy* 20:2–8
- [37] Buschow KHJ (1974) Calcium–nickel intermetallic compounds. *J Less Common Metals* 38:95–98
- [38] Saindrenan G, Vitart-Barbier J, Constantinoff M (1986) Structural study of nickel–calcium alloys containing between 0 and 15 wt% calcium. *J Less Common Metals* 118:227–333
- [39] Notin M, Belbacha D, Rahmane M, Hertz J, Saindrenan G, Jorda JL (1990) Experimental diagram and numerical optimization of the Ca–Ni system. *J Less Common Metals* 162:221–229
- [40] Uremovich D, Islam F, Medraj M (2006) Thermodynamic modelling of the Ca–Ni system. *Sci Technol Adv Mat* 7:119–126
- [41] Shinoda G (1928) Use of X-ray analysis to study the improvement of Al alloys (in Japanese). *Nippon Kogvo Kwai Shi* 44:544–562
- [42] Manyako NB, Zarechnyuk OS, Yanson TI (1987) Crystal structure of CaNiAl<sub>6</sub>. *Sov Phys Crystallogr* 32:816–817
- [43] Manyako NB, Yanson TI, Zarechnyuk OS (1988) Phase equilibria in the Ca–Co(Ni)–Al systems at 770 K. *Izv Akad Nauk SSSR Met* 3:185–187
- [44] Massalski TB (ed) (1990) *Binary alloy phase diagrams*, 2nd edn. ASM International, Metals Park
- [45] Villars P, Calvert LD (1991) *Pearson's handbook of crystallographic data for intermetallic phases*, 2nd edn. ASM, Materials Park
- [46] Viklund P, Haeussermann U, Lidin S (1996) NiAl<sub>3</sub>: a structure type of its own? *Acta Crystallogr A Found Crystallogr A* 52:C321
- [47] Gavra Z, Akiba E, Murray J, Calvert LD, Taylor JB (1985) Isotherms and crystallography of the hydrides of the system Ca<sub>x</sub>Eu<sub>1-x</sub>Ni<sub>5</sub>. *Mater Res Bull* 20:209–215
- [48] Oesterreicher H, Ensslen K, Kerlin A, Bucher E (1980) Hydriding behavior in Ca–Mg–Ni–B. *Mater Res Bull* 15:275–283
- [49] Dinsdale AT (1991) SGTE data for pure elements. *Calphad* 15:317–425
- [50] Redlich O, Kister AT (1948) Algebraic representation of thermodynamic properties and the classification of solutions. *Ind Eng Chem* 40:345–348
- [51] Blöchl PE (1994) Projector augmented-wave method. *Phys Rev B* 50:17953–17979
- [52] Kresse G, Joubert D (1999) From ultrasoft pseudopotentials to the projector augmented-wave method. *Phys Rev B* 59:1758–1775
- [53] Kresse G, Furthmüller J (1996) Efficient iterative schemes for ab initio total-energy calculations using a plane-wave basis set. *Phys Rev B* 54:11169–11186
- [54] Kresse G, Furthmüller J (1996) Efficiency of ab initio total energy calculations for metals and semiconductors using a plane-wave basis set. *Comput Mater Sci* 6:15–50
- [55] Perdew JP, Burke K, Ernzerhof M (1996) Generalized gradient approximation made simple. *Phys Rev Lett* 77:3865–3870
- [56] Perdew JP, Burke K, Ernzerhof M (1997) Emission in symmetric heavy ion reactions at subthreshold energies. *Phys Rev Lett* 78:1396
- [57] Monkhorst HJ, Pack JD (1976) Special points for Brillouin-zone integrations. *Phys Rev B* 13:5188–5192
- [58] Methfessel M, Paxton AT (1989) High-precision sampling for Brillouin-zone integration in metals. *Phys Rev B* 40:3616–3621
- [59] Sundman B, Jansson B, Andersson JO (1985) The thermo-calc databank system. *Calphad* 9:153–190
- [60] Chen SL, Daniel S, Zhang F, Chang YA, Yan XY, Xie FY, Schmid-Fetzer R, Oates WA (2002) The PANDAT software package and its applications. *Calphad* 26:175–188